Bull Volcanol (2014) 76:792
DOI 10.1007/s00445-013-0792-4

RESEARCH ARTICLE

Stratigraphy, chemistry, and eruptive dynamics of the 12.4 ka plinian eruption of Apoyeque volcano, Managua, Nicaragua

Denis Ramón Avellán · José Luis Macías · Giovanni Sosa-Ceballos · Gema Velásquez

Received: 16 February 2013 / Accepted: 10 December 2013 / Published online: 15 January 2014

Abstract Apoyeque volcano, located 9 km northwest of Managua city, erupted explosively at 12.4 ka. The Plinian eruption deposited a widespread pumice fall deposit known as the Upper Apoyeque Tephra (UAq). The UAq is massive, reversely graded, and consists of white juvenile pumice (~78 vol.%), a variety of cognate lithics and accidental altered lithics. The whole-rock pumice composition is rhyodacitic (SiO_2=66.9–68.5 wt.%) with a mineral paragenesis of plagioclase, orthopyroxene, clinopyroxene, amphibole, titanomagnetite, and ilmenite in a rhyolitic glass groundmass (SiO_2=74.4±0.6 wt.%). The deposit's dispersal axis is to the south, with the deposit covering a minimum area of 877 km^2 within the 50 cm isopach and has a total volume of 3 km^3 (dense rock equivalent, 1.15 km^3). The eruption column reached a maximum height of ca.28 km. The eruption ejected a total mass of 3×10^{12} kg at an average rate of 2×10^{8} kg/s, and based on available models, we infer duration of almost 4 h. Petrographic and geochemical characteristics suggest that the eruption was triggered by magma mixing.

Editorial responsibility: G. Giordano

Electronic supplementary material The online version of this article (doi:10.1007/s00445-013-0792-4) contains supplementary material, which is available to authorized users.

D. R. Avellán
Instituto de Geología y Geofísica, Universidad Nacional Autónoma de Nicaragua (IGG-CIGEO/UNAN-Managua), Managua, Nicaragua

D. R. Avellán (✉) · J. L. Macías · G. Sosa-Ceballos
Instituto de Geofísica, Unidad Michoacán, Universidad Nacional Autónoma de México, Ex-Hacienda de San José de La Huerta, C.P. 58190 Morelia, Michoacán, México
e-mail: denisavellan@gmail.com

G. Velásquez
Facultad de Ciencias e Ingeniería, Universidad Nacional Autónoma de Nicaragua, Managua, Nicaragua

Keywords Apoyeque volcano · Managua city · Plinian eruption · Eruptive dynamics

Introduction

Apoyeque stratovolcano is located about 9 km northwest of Managua city in the central–west region of Nicaragua. The volcanic edifice reaches an elevation of 430 m above sea level and belongs to the Central American Volcanic Arc. Volcanism in this region is linked to the subduction of the Cocos Plate beneath the Caribbean Plate along the Middle-America Trench, at an average rate of 70–90 mm/year (DeMets 2001) (Fig. 1). Apoyeque is one of 11 volcanic structures that form the Chiltepe Volcanic Complex at the northern end of the Nejapa Volcanic Field, all of which were emplaced during the Upper Pleistocene (Avellán et al. 2012) (Fig. 1). It is the only polygenetic volcano in this volcanic field, which includes at least 29 recognizable monogenetic structures emplaced along the N–S Nejapa fault (Avellán et al. 2012). The main Apoyeque cone consists of a stack of andesitic and dacitic lavas covered by dacitic pyroclastic deposits, with an approximate volume of 8 km^3 (Fig. 2).

Presently, Apoyeque is quiescent; however, future activity is expected because it is located in a seismo-tectonic intra-arc zone which has had many earthquakes during the past three decades (Walther et al. 2000). The eruptive record of the Chiltepe Volcanic Complex indicates that the complex has experienced six plinian eruptions since ca. 17 ka (Kutterolf et al. 2007) (Fig. 3). At least two of these eruptions, Lower Apoyeque and Chiltepe tephras, originated from the Apoyeque volcano (Freundt et al. 2006; Kutterolf et al. 2007). Few works have studied the UAq deposits (e.g., Bice 1985; Freundt et al. 2006; Kutterolf et al. 2007), and although it is thought that the UAq comes from the Chiltepe Volcanic Complex, none of these previous studies determined its precise source. Initially, Bice (1985) proposed Apoyeque volcano

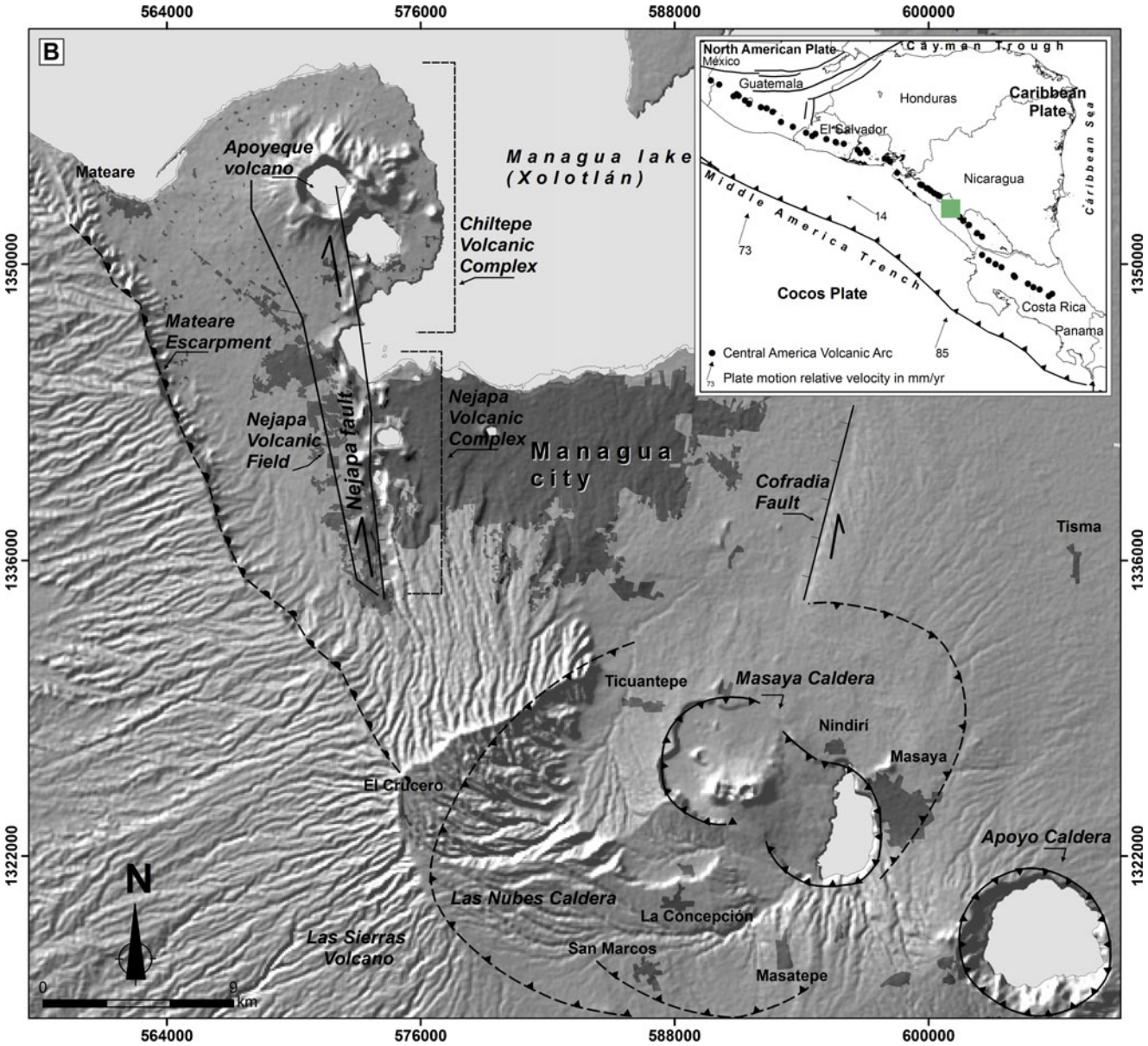

Fig. 1 Geological framework: **a** Regional tectonic setting showing the active subduction of the Cocos Plate beneath the Caribbean Plate that forms the Central America Volcanic Arc. *Green box* is the location of the Managua Graben; **b** Shape relief map of the Managua Graben with a 30-m resolution, showing volcanoes erupted along the Nejapa fault, and the active volcanoes Apoyo, Masaya, and the Chiltepe Volcanic Complex. *Dark-gray* polygons are populated areas and the studied area

as a probable source, considering the increasing thickness of UAq towards the peninsula of Chiltepe and found a dispersal axis to the south. Recently, Kutterolf et al. (2007) proposed that the UAq has a preferential dispersal axis to the west–northwest with a source located south of the Chiltepe Volcanic Complex at 1 km northwest of Managua, in the southwestern portion of the Xolotlán Lake (Fig. 1). Our study of the stratigraphy of the UAq clarifies the emission source, distribution, volume of ejected magma, and eruptive dynamics of this Plinian event. Finally, following petrographic and chemical analysis, we discuss some of the pre-eruptive conditions and potential triggering mechanisms of the eruption.

Analytical techniques

For this study, the UAq deposit was examined in 145 sites, out of which 44 were selected detailed stratigraphic sections (Fig. 4). These sections are located to the southeast, south, and west of the present Apoyeque crater up to a distance of 27 km (Fig. 4). In order to systematize the description of the UAq, we subdivided the deposit into five parts (a, b, c, d, and e) using section 9, located at the Acahualinca site (Fig. 4), as a reference. In order to determine the vertical and lateral granulometric variations of UAq, we collected 15 samples

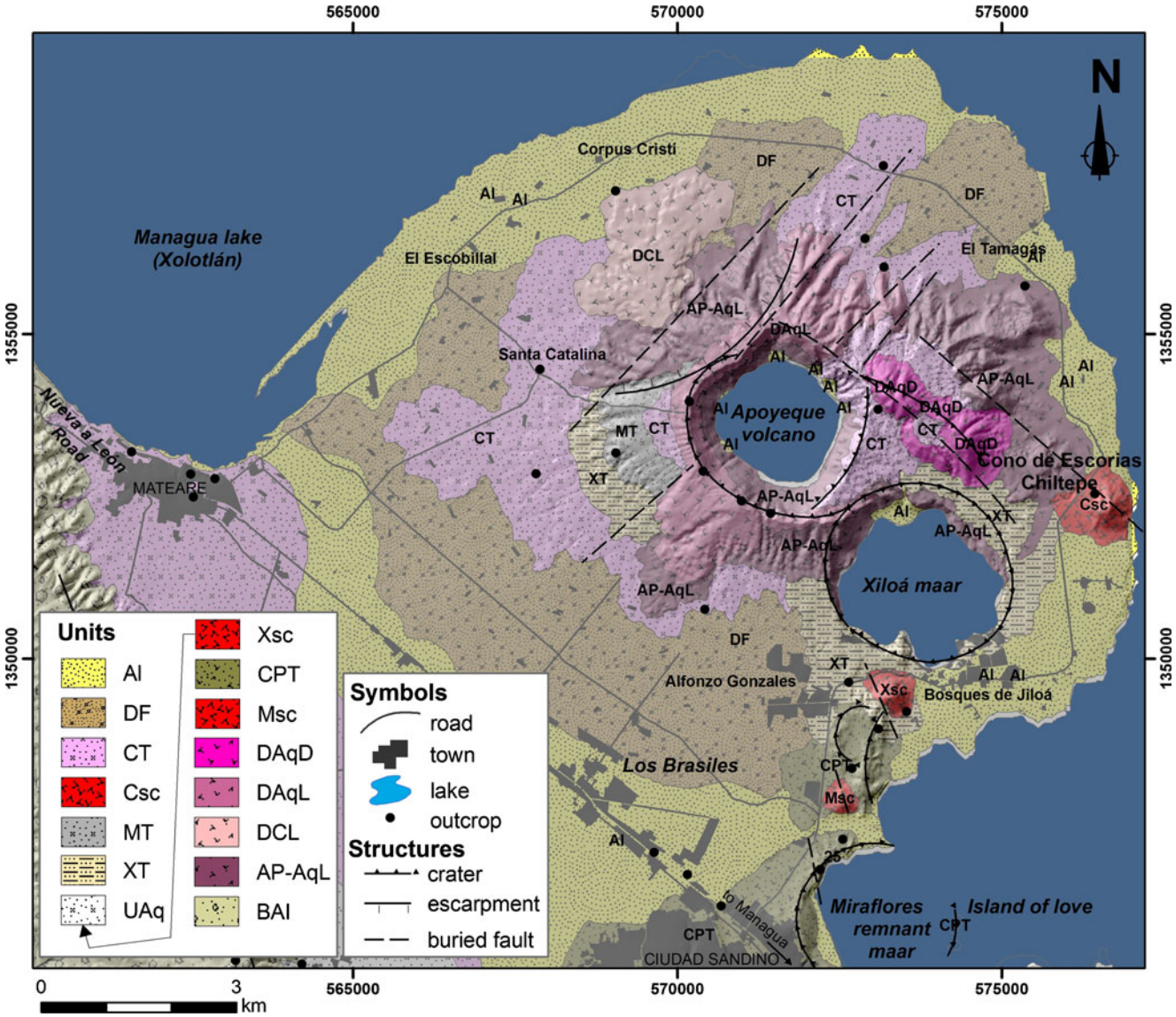

Fig. 2 Geological map of the Chiltepe Volcanic Complex. Notice the Apoyeque volcano and the distribution of main lithological units identified. The southern outskirts of Apoyeque volcano are covered with Holocene pyroclastic deposits. Roads and infrastructure are located atop these pyroclastic deposits. Key for lithology: *BAI*, Basaltic Andesite Ignimbrite; *AP-AqL*, Andesitic Pre-Apoyeque lavas; *DCL*, Dacitic corpus lavas; *DAqL*, Dacitic Apoyeque lavas; *DAqD*, Dacitic Apoyeque domes; *Msc*, Miraflores scoria cone; *CPT*, Cuesta El Plomo Tuff; *Xsc*, Xiloá scoria cone; *UAq*, Upper Apoyeque Tephra; *XT*, Xiloá Tephra; *MT*, Mateare Tephra; *Csc*, Chiltepe scoria cone; *CT*, Chiltepe Tephra; *DF*, Debris flow; and *Al*, alluvial

along the dispersal axis of the deposit at sections 9, 11, and 15 (Fig. 4). These sections are located at 9, 14.2, and 18.3 km from the source with deposit thicknesses of 460, 270, and 190 cm, respectively. At each section, we collected samples from each recognized stratigraphic level (a–e levels), each one containing 1 to 2 kg of material. Samples were dry-sieved at 1 pre-harvest interval (phi) between −5 and 3 phi. Granulometric statistical parameters (Md phi and σphi) were calculated for each sample by using Kware software (Wohletz 2006) and Inman (1952) parameters. Five samples collected at site 9 were used for componentry analyses by counting more than 600 particles per sample. We repeated at least ten counts of each sample and found errors of less than ±0.2 vol.%.

The average density and vesicularity of pumice was measured in the different UAq levels from −4 and −3 phi clast sizes. A total of 298 clasts were measured (a=44, b=71, c=56, d=68, and e=59). The density of each clast was analyzed using the water immersion technique of Houghton and Wilson (1989) and Gardner et al. (1996).

Twelve pumice samples were collected to prepare polished sections (site 9) (Fig. 4). Analyses of minerals and glass were carried out on an electron microprobe JEOL model JXA8900-

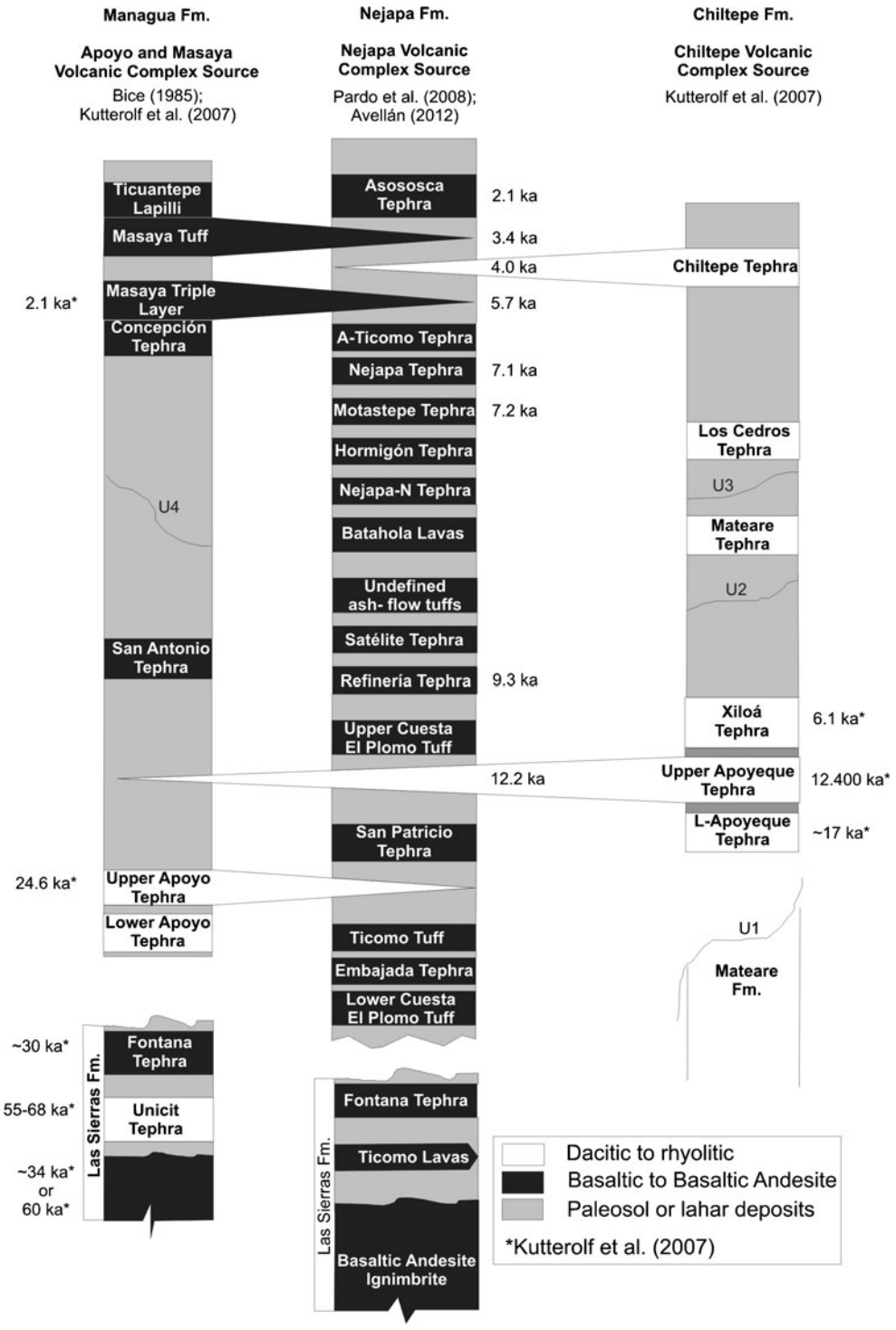

Fig. 3 Stratigraphic correlation of tephra successions in the Managua Graben produced by Apoyo, Masaya, Chiltepe, and Nejapa volcanic complexes during the past ca. 40 ka. The *left* and *right columns* show the tephra sequences of Bice (1985) and Kutterolf et al. (2007), respectively. The *central column* summarizes the stratigraphy of Nejapa, Chiltepe, and Managua formations of Pardo et al. (2008) and Avellán et al. (2012). The UAq unit is interbedded with the Nejapa, Chiltepe, and Managua formations. Major erosional unconformities are indicated as *U1* to *U4* (Kutterolf et al. 2007)

R of the Instituto de Geofísica of the Universidad Nacional Autónoma de México. The analytical conditions used were: an acceleration voltage of 20 kv and a focused beam current of 20 nA for most minerals except hornblende. For the analyses of glass and hornblende, we used an unfocused beam of 5 to 10 microns, to avoid loss of water and Na migration, respectively.

Stratigraphy of the UAq

Stratigraphic relationships

The UAq is a fall deposit that has been used as a stratigraphic marker in the Managua area. UAq is interbedded with volcanic deposits from other volcanoes, such as Chiltepe, Nejapa,

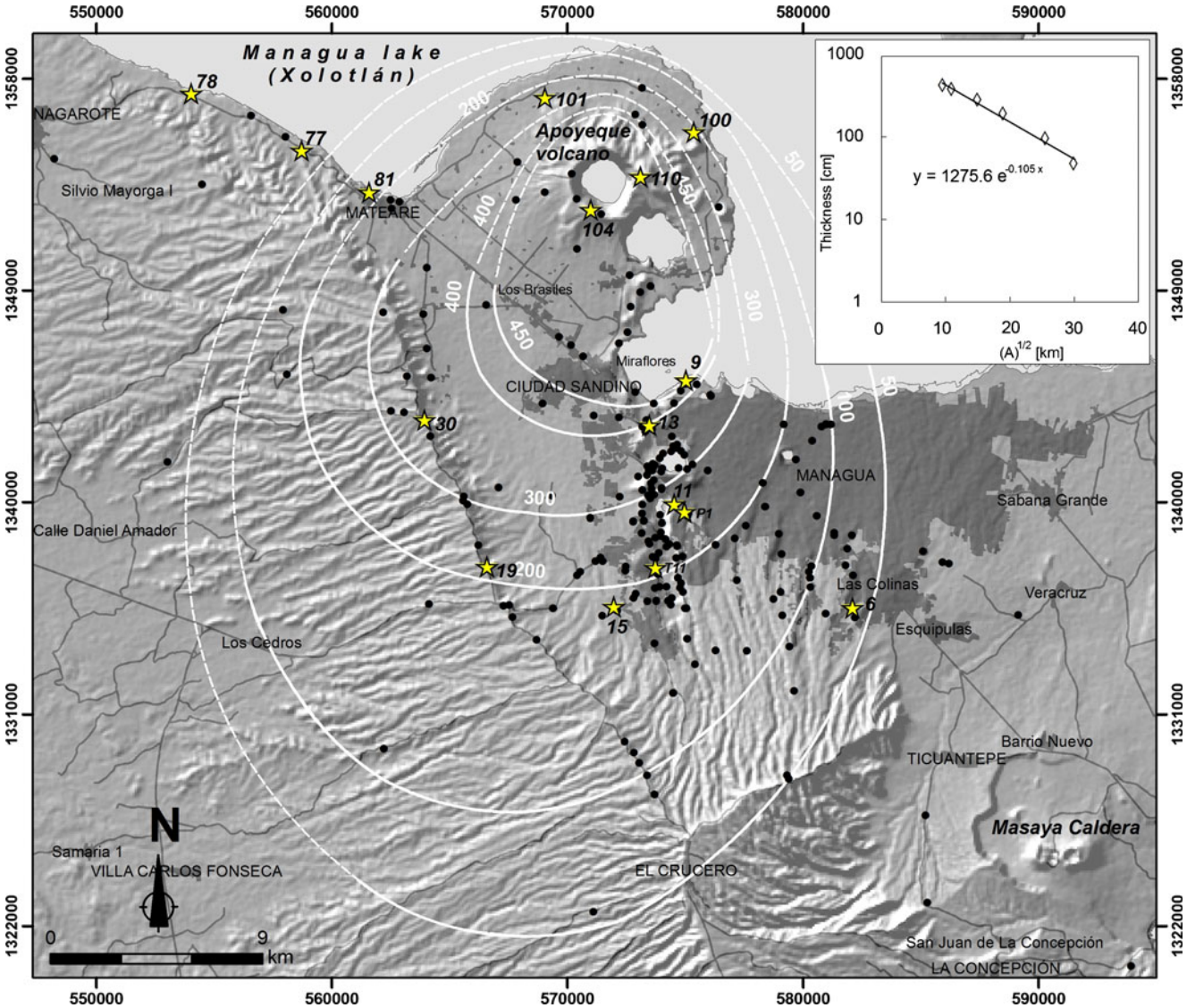

Fig. 4 Isopach map of the UAq (contour lines are in centimeters) with the location of stratigraphic profiles. *Stars with numbers* indicate sites mentioned in the text. Diagram of the square root of the isopach area (√A) versus thickness of the UAq deposit (Pyle 1989, 1995)

Masaya, and Apoyo Caldera (Fig. 1). The late Pleistocene–Holocene activity of these volcanic centers blanketed the Managua area many times, producing a complex volcanic stratigraphy (Fig. 3). These strata have been divided into four main formations: Las Sierras, Chiltepe, Nejapa, and Managua (Bice 1985; Freundt et al. 2006; Kutterolf et al. 2007; Avellán et al. 2012) (Fig. 3). The UAq is one of the six tephra units of the Chiltepe Formation.

In most outcrops, UAq is in contact with various deposits of the formations mentioned above, separated by paleosols at locations described south of Managua and within the city. For instance, at section 6 (Fig. 4), UAq covers a paleosol developed on top of the Upper Apoyo Tephra with a maximum age of 24,650±120 years before present (BP) (sourced at Apoyo Caldera, base of the Managua Formation) and underlies the Masaya Triple Layer with a maximum age of 5,755±90 years BP (sourced at Masaya Caldera, Managua Formation) (Fig. 5). Inside the eastern slope of the Nejapa Maar, UAq overlies a paleosol developed on top of the Fontana Tephra of ca. 30 ka (Las Sierras Formation) (Figs. 4 and 5; section 11). To the east of the Nejapa Maar UAq directly overlies the San Patricio cinder cone (Nejapa Formation) (Figs. 4 and 5; section P1). South of Nejapa and over the Ticomo Maar and surrounding areas, the UAq underlies lahar deposits that originated from the southern part of the Managua graben on the Mateare escarpment. West of Managua, UAq is covered by the Nejapa Tephra with a maximum age of 7,135±125 years BP (Nejapa Formation) with an erosive contact (Figs. 4 and 5; section 15). Northwest of Managua, at the Cuesta El Plomo volcanic complex, it is bracketed by the Lower and Upper Cuesta El Plomo Tuffs (Nejapa Formation) (Figs. 4, 5, and 6a–b; section 9). On the Mateare escarpment, UAq is covered

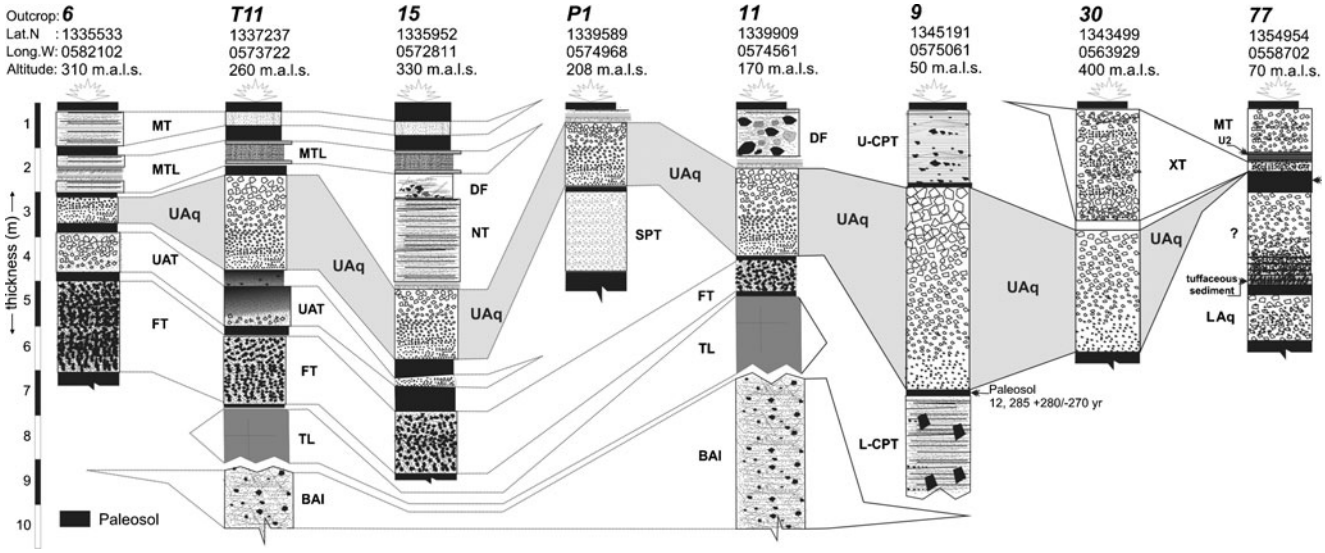

Fig. 5 Correlation of the key stratigraphic outcrops of the UAq. Key for deposits: *BAI*, basaltic andesite ignimbrite; *TL*, Ticomo lavas; *FT*, Fontana Tephra; *L-CPT*, Lower Cuesta El Plomo Tuff; *UAT*, Upper Apoyo Tephra; *LAq*, Lower Apoyeque Tephra; *SPT*, San Patricio Tephra; *UAq*, Upper Apoyeque Tephra; *U-CPT*, Upper Cuesta El Plomo Tuff; *NT*, Nejapa Tephra; *XT*, Xiloá Tephra; *U2*, erosional unconformities; *MT*, Mateare Tephra; *DF*, Debris flow; *MTL*, Masaya triple layer; *MT*, Masaya Tuff

by the Xiloá Tephra with a maximum age of 6,105±30 years BP (Chiltepe Formation) (Figs. 4 and 5; section 19 and 30). However, at sections located around the Mateare village (e.g., in 77, 78, and 81 sections; Fig. 4), 10 km southwest of Apoyeque, the UAq fallout was eroded by pyroclastic surges of the Xiloá eruption.

Age of the deposit

The UAq deposit was first dated by Kutterolf et al. (2007) who obtained a ^{14}C age of 12,400±100 years BP of a paleosol underneath the deposit. In this work, two new ^{14}C ages were determined on the paleosol underneath the UAq deposit in different locations. From both sites, we collected the topmost five centimeters of the paleosol. These samples were analyzed by the ^{14}C standard radiometric method at the Laboratory of Isotope Geochemistry (Arizona University Tucson, USA) whose results are reported in Table 1 as conventional dates in years BP. The first paleosol (160 cm thick) is a clayey, humic-rich, dark-brown paleosol collected at site 9 (9 km southeast of present Apoyeque volcano crater at Acahualinca) (Figs. 4 and 6, Table 1). The paleosol was developed from the Lower Cuesta El Plomo Tuff and is overlain by 4.6 m of the UAq deposit. The conventional ^{14}C age for this paleosol was 12,285+280/−270 years BP. The second sample (15 cm thick) is a silty-clayey, humic-poor, light-brown paleosol collected in a road cut at site Cuesta El Plomo northwest of the city of Managua (Fig. 4, Outcrop-13, Table 1). The paleosol is covered by only 20 cm of the UAq deposit, which was strongly eroded by the Upper Cuesta El Plomo Tuff. The age obtained from this paleosol is 10,145+295/−285 years BP. Only the paleosol at Acahualinca

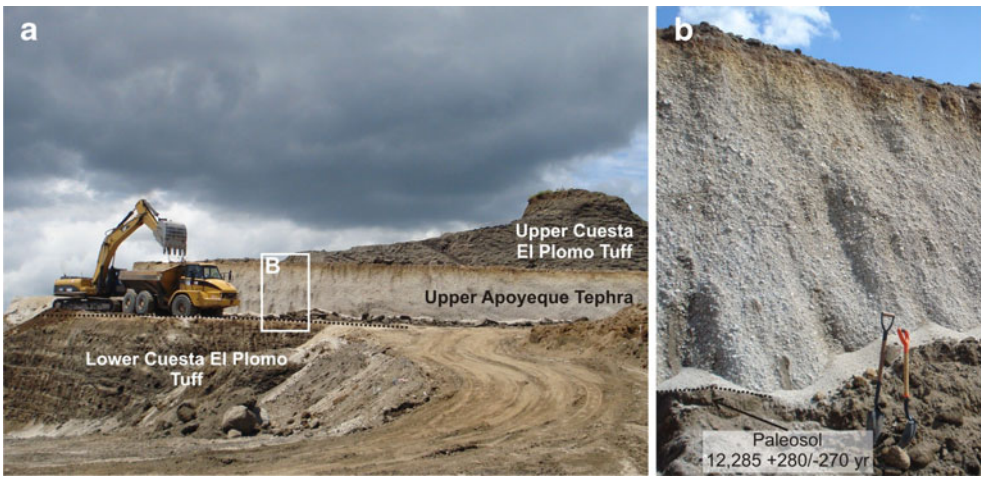

Fig. 6 Photographs of: **a** *Gray* planar-stratified phreatomagmatic base-surge deposits forming the Lower Cuesta El Plomo Tuff, overlain by the white, massive, pumice fallout of the UAq and by the *gray* planar-stratified base-surge deposits of the Upper Cuesta El Plomo Tuff, as exposed northwest of Managua city (Acahualinca quarry, site 9); **b** aspect of reversely graded facies of the UAq deposit above the paleosol developed from the Lower Cuesta El Plomo Tuff

Table 1 Radiocarbon dates of paleosol samples performed during study. The locations are in UTM coordinates

Outcrop	Description (sample)	Location North	West	Lab. code	Conventional age years BP	$\delta^{13}C$ (‰)
9	Paleosol below UAq	1345191	575061	A-14267	12, 285 +280/−270	−14.1
13	Paleosol below UAq	1343450	573354	A-14264	10, 145 +295/−285	−18.1

compares well with the age reported by Kutterolf et al. (2007). The second sample yielded a younger age, probably due to paucity of organic matter in the horizon. Therefore, the age of the UAq eruption is thus fairly well-constrained around 12.4 ka.

Description of the deposit

In most exposures, the UAq appears as a single massive, white, framework-supported layer with reverse grading (Figs. 4, 5, and 6a–b). UAq is preserved as a 4.6 m thick deposit at Acahualinca (section 9) located at 9 km southeast of the Apoyeque crater (Figs. 4 and 6a–b). The UAq has a minimum thickness of 50 cm at Sierras Santo Domingo and Las Colinas (section 6) located at 22 km southeast of the crater (Fig. 4). The UAq tephra shows marked southward dispersal (Fig. 4). The UAq consists mainly of white angular to subangular pumice and three types of lithic clasts (angular red, ochre, and rounded gray lava). These lithics are reversely graded through the deposit; they increase in concentration and size above the middle portion of the deposit and disappear toward the top.

We divided the UAq deposit into five different parts (from bottom a to top e) described at section 9 as follows: part a, the lower level consists of white, subangular pumice with coarse ash, ochre, and rare gray lava lithics: Pumice clasts have subspherical vesicles and a few plagioclase, pyroxene, amphibole, and Fe-Ti oxide phenocrysts; part b, this level contains white, subangular fine lapilli pumice with subspherical vesicles and has slightly fewer red and gray lava lithics; part c, this level contains white, subangular coarse lapilli pumice with slightly more abundant in gray rounded and red-ochre hydrothermally altered lava lithics: Pumice clasts show elongated to ellipsoidal vesicles; part d, this level contains white, subangular pumice lapilli with a marked increase in gray-to pink and ochre hydrothermally altered lithics: Pumice clasts show spherical to elongated vesicles; part e, the uppermost level has white subangular lapilli to block-sized pumice, and rare lithics: Pumice is fibrous and has elongated vesicles with glomeroporphyritic texture and a mineral assemblage of plagioclase, pyroxene, and Fe-oxide phenocrysts.

Granulometry

UAq has a unimodal grain-size distribution that varies with distance from the crater and vertically through the unit. Vertical variations in the deposit were studied at proximal (site 9, at 9 km) and intermediate (site 11, 14.2 and site 15,

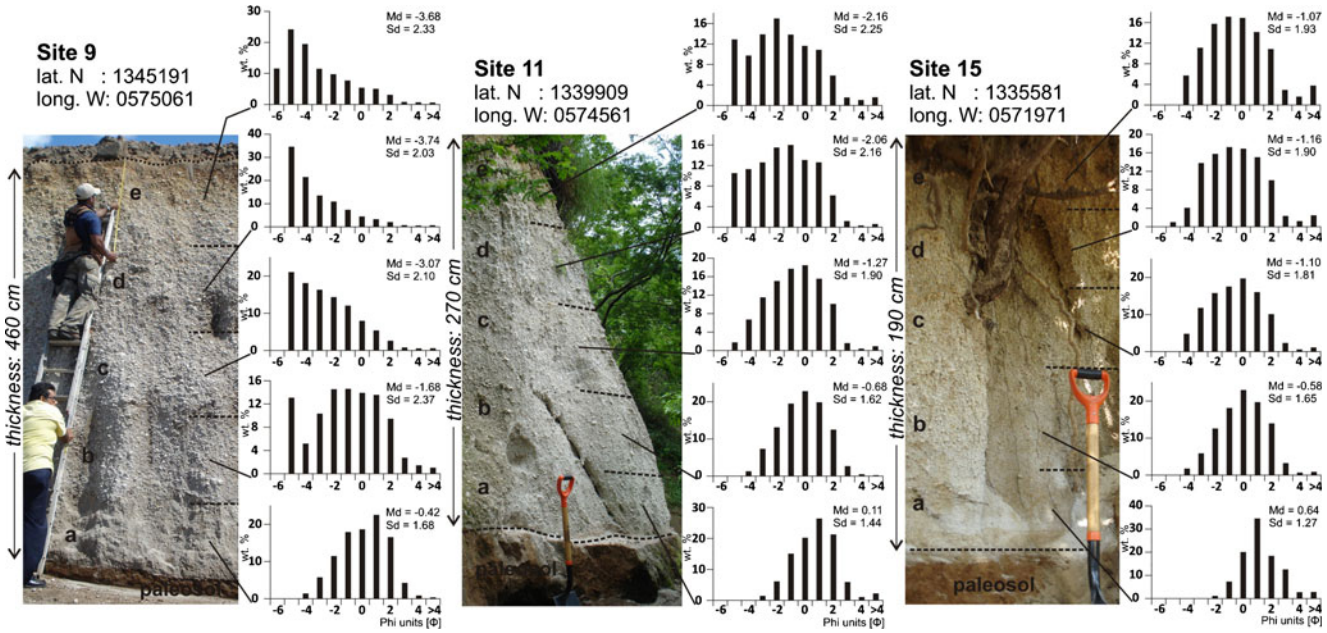

Fig. 7 View of UAq exposures along the dispersal axis with increasing distance from the source. *Lines* indicate sampling sites (levels a–e) and their respective granulometric distributions

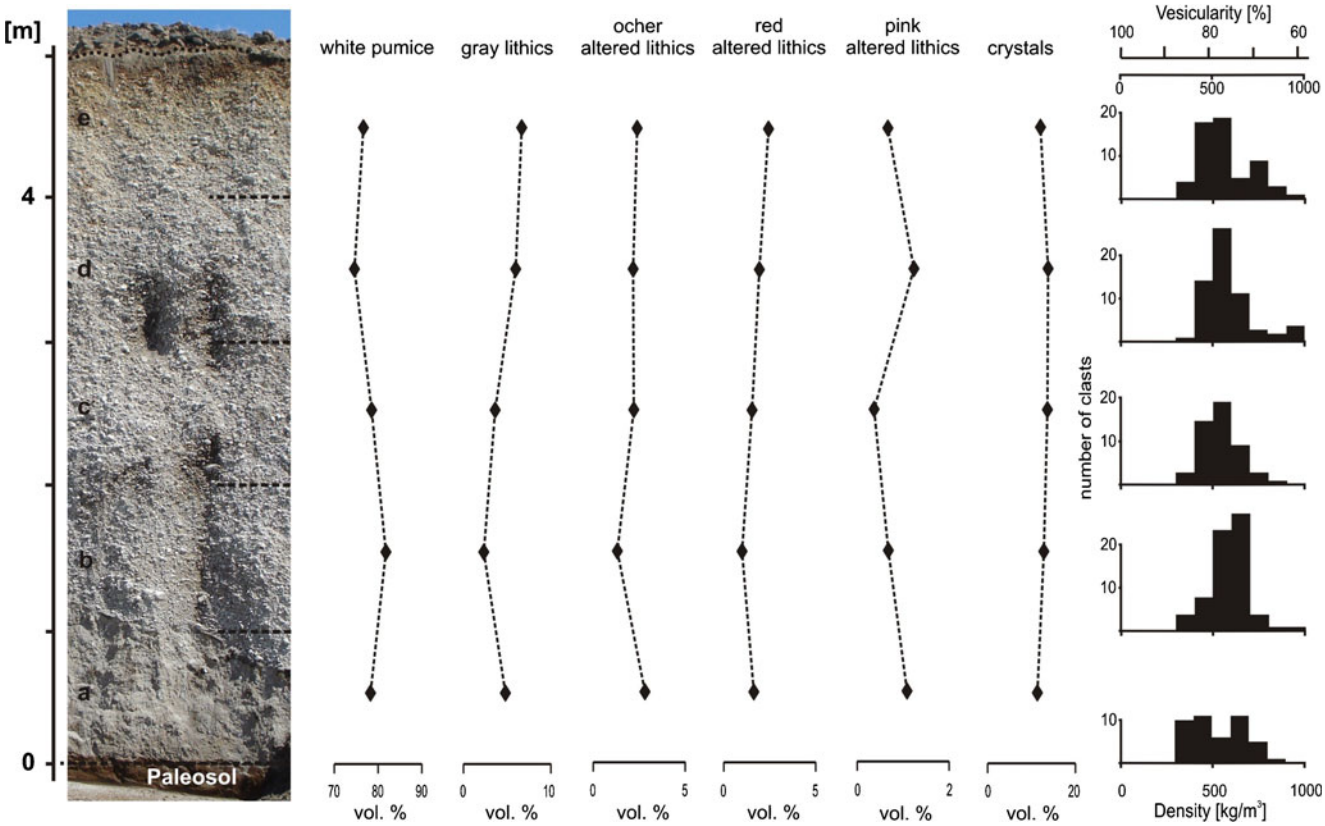

Fig. 8 Composite stratigraphic section of UAq at site 9 showing the histogram distributions of pumice (clast density and vesicularity) of levels a–e. To the *center* appears the vertical component variations showing a clear vertical decrement of pumice contrasting with an increasing of accidental and old lithic clasts to the top

18.3 km) distances from the volcano along the dispersal axis (Figs. 4 and 7). In proximal sections (e.g., 9), UAq has a main mode that varies from +1ϕ (a) at the base to −5ϕ (c–e) in upper levels. Level-b shows a secondary mode at −5ϕ that reflects the presence of ballistic blocks. Intermediate sections at 14.2 km (e.g., site 11) and 18.3 km (e.g., site 15) also show reverse grading of the deposit. In addition, UAq is finer and becomes better sorted with distance from vent (Fig. 7).

Componentry

In order of abundance, the UAq deposit consists of white pumice, cognate variably altered lithics (gray, red, and pink), accidental altered lithics (ochre), and loose crystal fragments (plagioclase, pyroxene, amphibole, and Fe-Ti oxide) (Fig. 8). Noteworthy is that UAq has an average of 78 vol.% white pumice throughout the deposit while cognate and accidental lithics have variable concentrations under 12 vol.%.

Density and vesicularity

Density of white pumice fragments is fairly homogeneous throughout UAq stratigraphic levels, varying from 539±146 to 595±105 kg/m^3 (average density of 569±124 kg/m^3) (Fig. 8). Such densities correspond to total vesicularities ranging from 77±4 to 79±6 % (average vesicularity index following Houghton and Wilson (1989) is 78±5 %). These high vesicularity values of white pumice fragments coincide with the minimum theoretical values necessary for magma fragmentation during a plinian eruption of 75 % (Sparks 1978), 71 % (Houghton and Wilson 1989), and 64 % (Gardner et al. 1996).

Petrography

Polished sections were prepared for five pumice samples of the UAq deposit (section 9), one for each level (a–e). Six additional rock samples were collected from different units of the Apoyeque stratovolcano (Fig. 2) and four accidental lithic fragments from the UAq deposit to interpret lithic contributions to the UAq deposit from the older lava flows of Apoyeque volcano.

UAq pumice is in thin section homogeneously vesicular (dominated by semi-circular to slightly elongated shapes) with some patches of apparently fibrous texture. Pumice clasts of UAq have porphyritic, hypohyaline, and highly vesicular textures with 4 % phenocrysts set in a glassy groundmass (18 %), and abundant vesicles (78 %). The mineral

Table 2 Whole-rock analyses of juvenile samples of Apoyeque volcano and the 12.4 kyears BP (UAq)

Sample	A4	A3	A2	A1	Ch	Xi	e	d	c	b	a	e′	d′	c′	b′	a′
Outcrop	110	104	101	100	99	96	9	9	9	9	9	9	9	9	9	9
Rock type	Lava	Lava	Lava	Lava	Scoria	Scoria	Pumice	Pumice	Pumice	Pumice	Pumice	Pumice	Pumice	Pumice	Pumice	Pumice
Lat. N	1354384	1352463	1357228	1355781	1352563	1349220	1345191	1345191	1345191	1345191	1345191	1345191	1345191	1345191	1345191	1345191
Long. W	572967	570971	569025	575337	576409	573516	575061	575061	575061	575061	575061	575061	575061	575061	575061	575061
Major elements (wt.%)																
SiO_2	67.37	64.93	64.4	61.52	53.02	48.65	66.9	67.4	67.18	67.41	67.37	68.18	68.03	68.23	68.5	67.4
Al_2O_3	15.9	15.86	15.76	16.42	17.51	16.92	13.54	13.81	14.65	14.04	13.58	13.82	14.24	14.17	14.04	14
Fe_2O_3	4.27	5.43	6.86	7.51	10.73	11.12	5.18	3.45	4.29	3.32	3.45	3.37	3.43	3.32	3.08	3.44
MnO	0.072	0.167	0.188	0.142	0.192	0.191	0.101	0.1	0.105	0.097	0.098	0.102	0.103	0.103	0.096	0.102
MgO	1.12	1.39	1.55	1.98	4.95	8.32	0.86	0.88	0.99	0.72	0.69	0.88	0.86	0.85	0.73	0.8
CaO	3.44	4.33	4.65	5.33	9.85	12.5	3.13	3.26	3.43	3.06	2.99	3.23	3.36	3.24	3.34	3.32
Na_2O	4.52	4.41	4.61	3.61	2.77	2.4	3.79	3.81	3.74	3.8	3.76	3.78	3.77	3.76	3.8	3.75
K_2O	2.07	2.11	1.74	2	0.77	0.49	2.32	2.3	2.24	2.35	2.39	2.25	2.24	2.29	2.3	2.27
TiO_2	0.474	0.596	0.756	0.68	0.786	0.838	0.293	0.286	0.31	0.287	0.28	0.299	0.311	0.307	0.291	0.304
P_2O_5	0.17	0.2	0.3	0.16	0.15	0.15	0.07	0.07	0.11	0.06	0.07	0.1	0.11	0.1	0.09	0.11
LOI	1.54	1.26	−0.32	1.23	−0.25	−0.59	4.13	4.43	3.7	4.32	4.33	4.73	4.23	4.29	4.45	4.46
Total	100.9	100.7	100.5	100.6	100.5	101	100.3	99.79	100.7	99.47	99.02	100.7	100.7	100.7	100.7	99.98

All samples were analyzed in the Activation Laboratories (Actlabs), Ancaster, Canada using inductively coupled plasma mass spectrometry and instrumental neutron activation analysis for major and trace elements

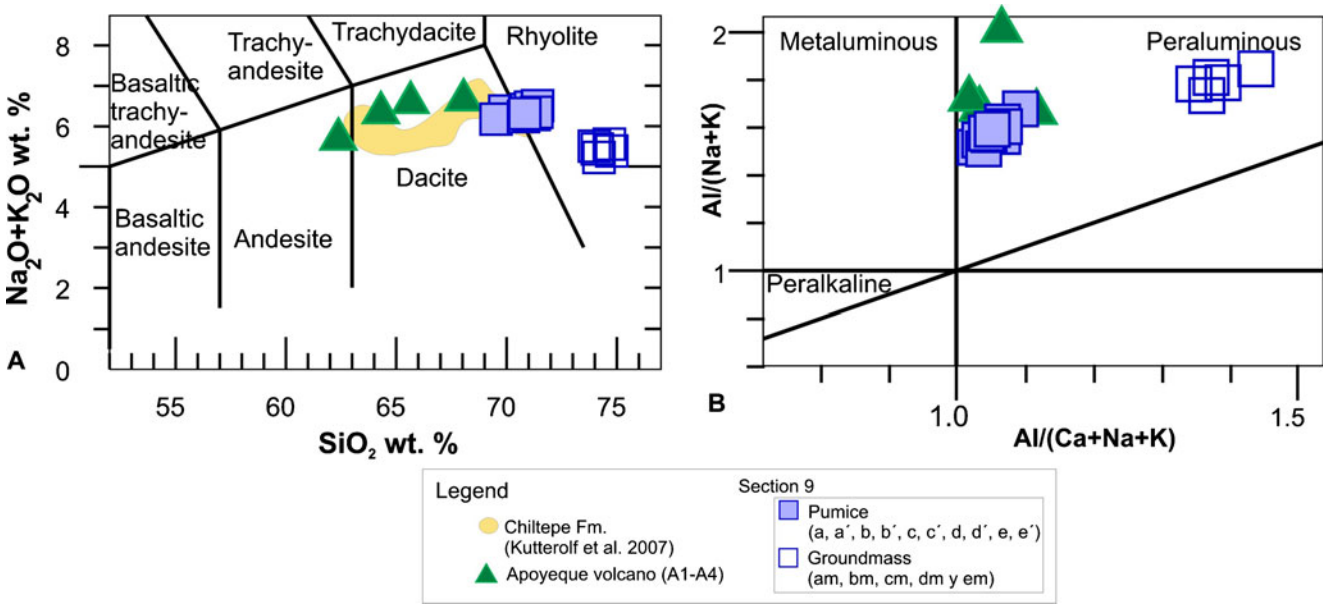

Fig. 9 **a** Total alkalis (Na_2+K_2O) versus SiO_2 diagram for volcanic rocks (date of Table 2), normalized to anhydrous basis, including the data of Kutterolf et al. (2007); **b** all studied rocks fall in the peraluminous field considering the alumina saturation index of Shand (1951)

assemblage includes plagioclase (2.3 %), orthopyroxene (0.9 %), clinopyroxene (0.6 %), amphibole (0.8 %), Fe-Ti oxides (<0.4 %), and apatite as accessory mineral. Crystals are hypidiomorphic with subhedral and anhedral shapes. Glomerocrysts appear in level-c, increasing in concentration to level-e.

The gray cognate lithics of the UAq and the basal lavas of Apoyque have a similar mineral assemblage with plagioclase, olivine, orthopyroxene, clinopyroxene, and Fe-Ti oxides set in a microlitic groundmass of the same minerals and glass. The red and pink altered lithics have the mineral association as the younger lavas and domes of Apoyeque with plagioclase, orthopyroxene, clinopyroxene, Fe-Ti oxides, and sanidine and amphibole as accessory minerals embedded in a microlitic groundmass of plagioclase and glass. In contrast, the ocher accidental altered lithics have a phaneritic texture with plagioclase, quartz, orthoclase, biotite, Fe-Ti oxides, and accessory zircon, typical of a granodiorite.

Chemistry

Fourteen whole-rock analyses were carried out, including ten pumice samples of the UAq deposit (section 9), two of each level (*a-e* and *a´-e´*) and four lava samples from the Apoyeque stratovolcano (Figs. 2 and 4, Table 2). Ten pumice samples were collected to prepare polished sections and mineral separations.

Compositions

Apoyeque volcano rocks vary in composition from andesite at the base of the volcano to dacite at the top (Fig. 9) and range in silica content from 61.5 to 67.4 wt.% and Fe_2O_3 from 4.2 to 7.5 wt.% (Table 2). Pumice from section 9 (UAq, Acahualinca) is rhyodacitic with silica contents of 66.9–68.5 wt.% (Fig. 9a) and peraluminous (Fig. 9b).

The binary diagrams show that rocks from the Apoyeque edifice are more ferromagnesian than pumice from section 9 (Fig. 10). There is a negative correlation of FeO, MgO, CaO, and TiO_2 oxides with silica. K_2O displays a gradual increase with increasing silica (Fig. 10).

Matrix glass compositions

The groundmass glass of UAq pumice in section 9 is rhyolitic and compositionally uniform (SiO_2=74.4±0.6 wt.%) (Fig. 11; ESM 1). The K_2O content of pumice is heterogeneous and does not show any systematic difference. The FeO increases with CaO (Fig. 11).

Mineral composition

Plagioclase

The most abundant crystal phase in UAq pumice (ESM 2), plagioclase, occurs as tabular subhedral to anhedral phenocrysts and microphenocrysts (<2 mm in size). It has combined albite and Carlsbad twins. Some crystals contain Fe-Ti oxide micro-inclusions and glass inclusions. Three main types of crystals are observed. The first consists of unzoned crystals with composition between An_{42} and An_{55} (Fig. 12a). The second is crystals with calcic cores (~An_{84}) and more evolved rims (~An_{45}). The third comprises crystals with calcic rims (~An_{83}) that overgrew more evolved cores (~An_{43}).

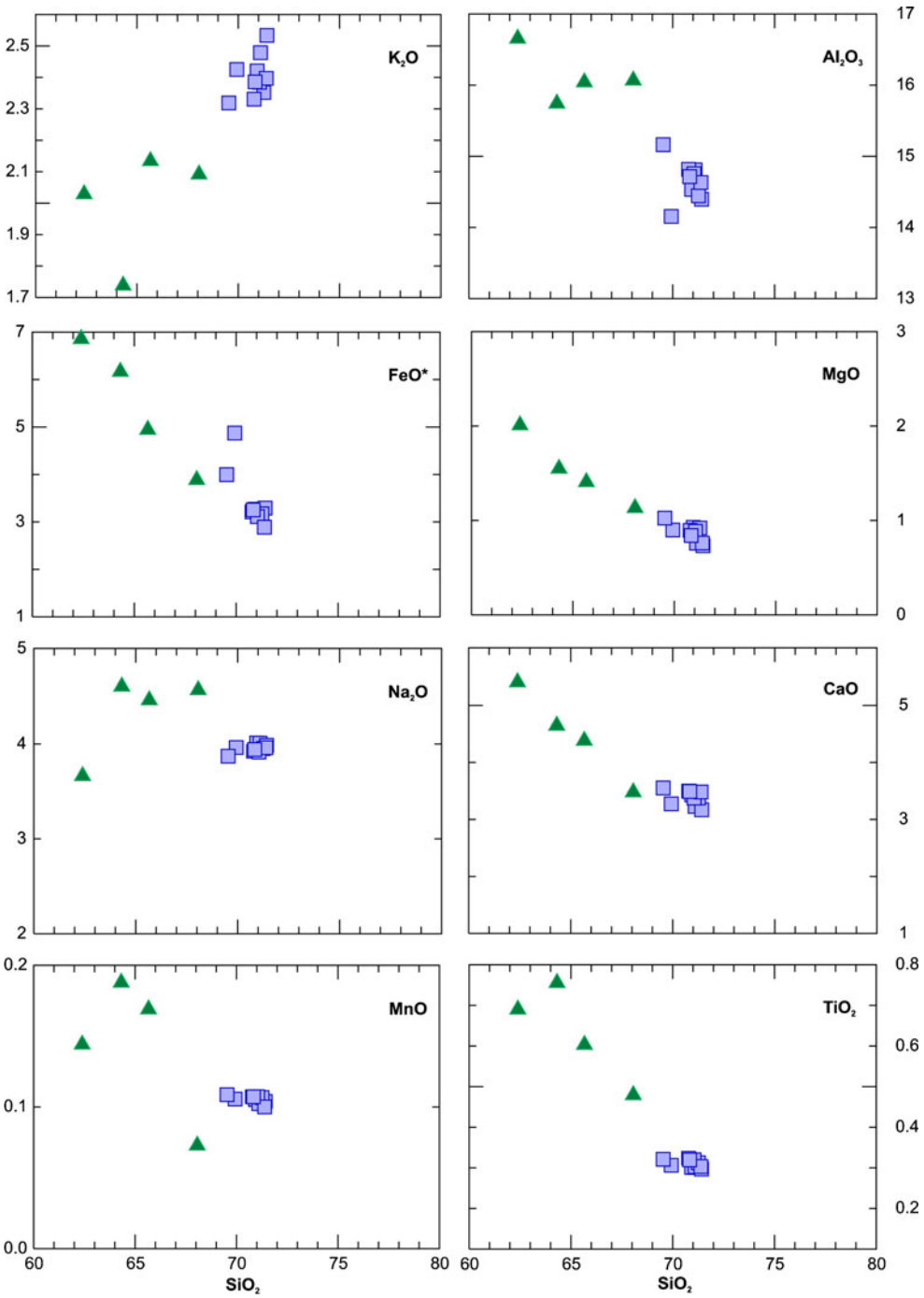

Fig. 10 Binary diagrams of some major elements of the studied samples

Pyroxene

The most common ferromagnesian minerals are pyroxenes, both orthopyroxene and clinopyroxene (ESM 3). Pyroxenes appear as phenocrysts and microphenocrysts (<1 mm in size) with prismatic–tabular forms and subhedral to anhedral shapes commonly containing Fe-Ti oxide micro-inclusions. The orthopyroxene is brown with compositions of En_{55-65}, Fs_{33-43}, Wo_{2-3}, and Mg#=42–52 (Mg#=((Fetot+Mg)/Mg)×100) composition (Fig. 12b). Clinopyroxene has prismatic shapes, greenish color and limited compositional range (En_{38-41}; Wo_{43-45}; Mg#=54–59).

Amphibole

Phenocrysts and microphenocrysts (<1 mm in size) of amphibole are dark green, tabular, with subhedral to anhedral shapes (ESM 4). Some crystals contain Fe-Ti oxide micro-inclusions.

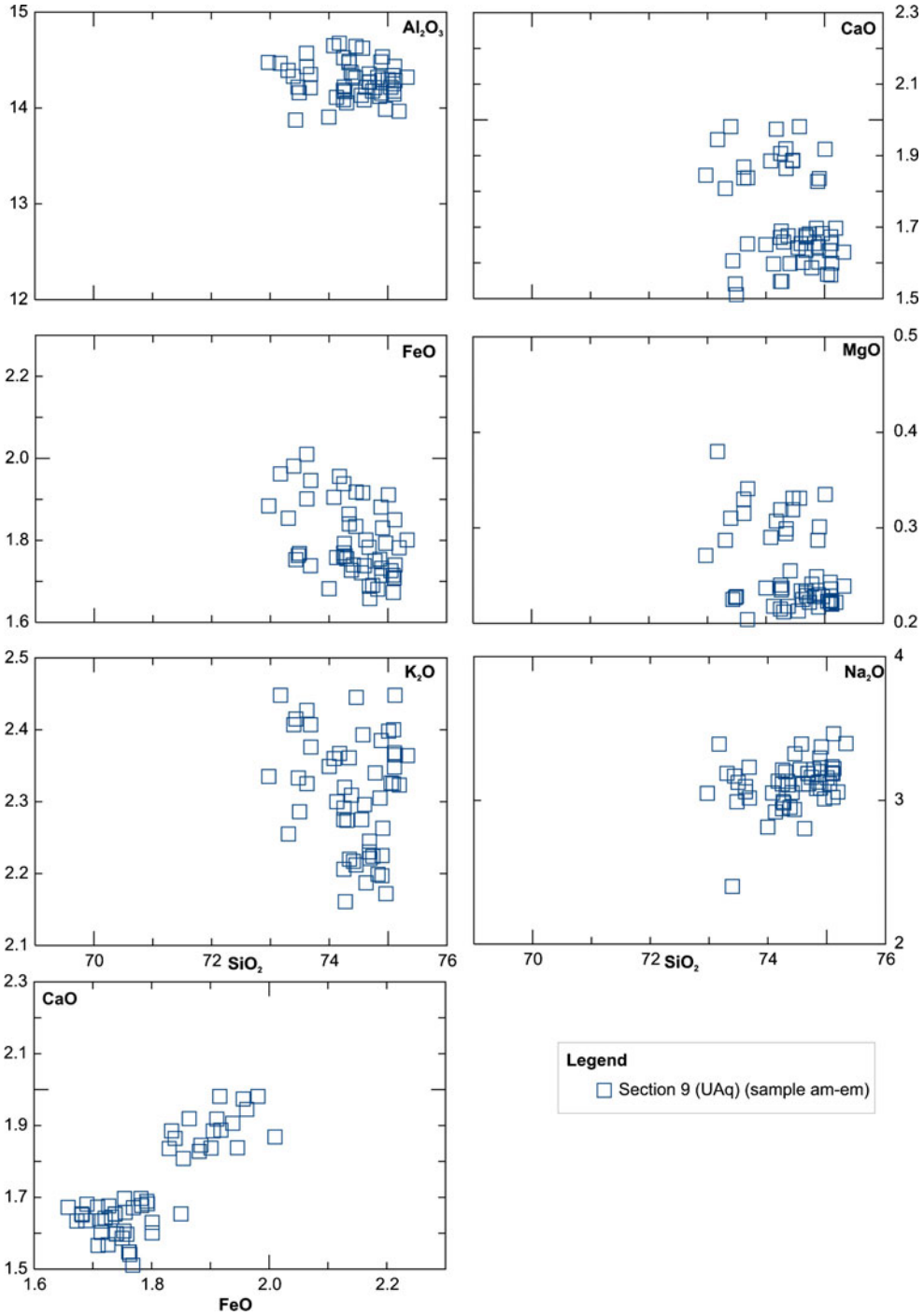

Fig. 11 Major oxide glass composition of UAq pumice collected at section 9 (Acahualinca). The data represents individual glass electron microprobe analysis. It is clear that two groups of glass compositions occur

The population of amphiboles is compositionally homogeneous (e.g., TiO_2=1.8±0.07 wt.%; Al_2O_3=8.0±0.3 wt.%).

Fe-Ti oxides

Titanomagnetite and ilmenite are present in the UAq pumice (ESM 5). Titanomagnetite is present as microphenocrysts (<500 μm in size), subhedral to anhedral shapes, disseminated in the groundmass and as inclusions in plagioclase, pyroxene, and amphibole phenocrysts. The phenocrysts of titanomagnetite have $Usp_{28.6\pm0.2}$, but differences in Al_2O_3, MgO and TiO_2 allow definition of two groups (Fig. 12c–d). The crystals of ilmenite are much less abundant than those of titanomagnetite and show a compositional range of $Ilm_{84\pm0.4}$.

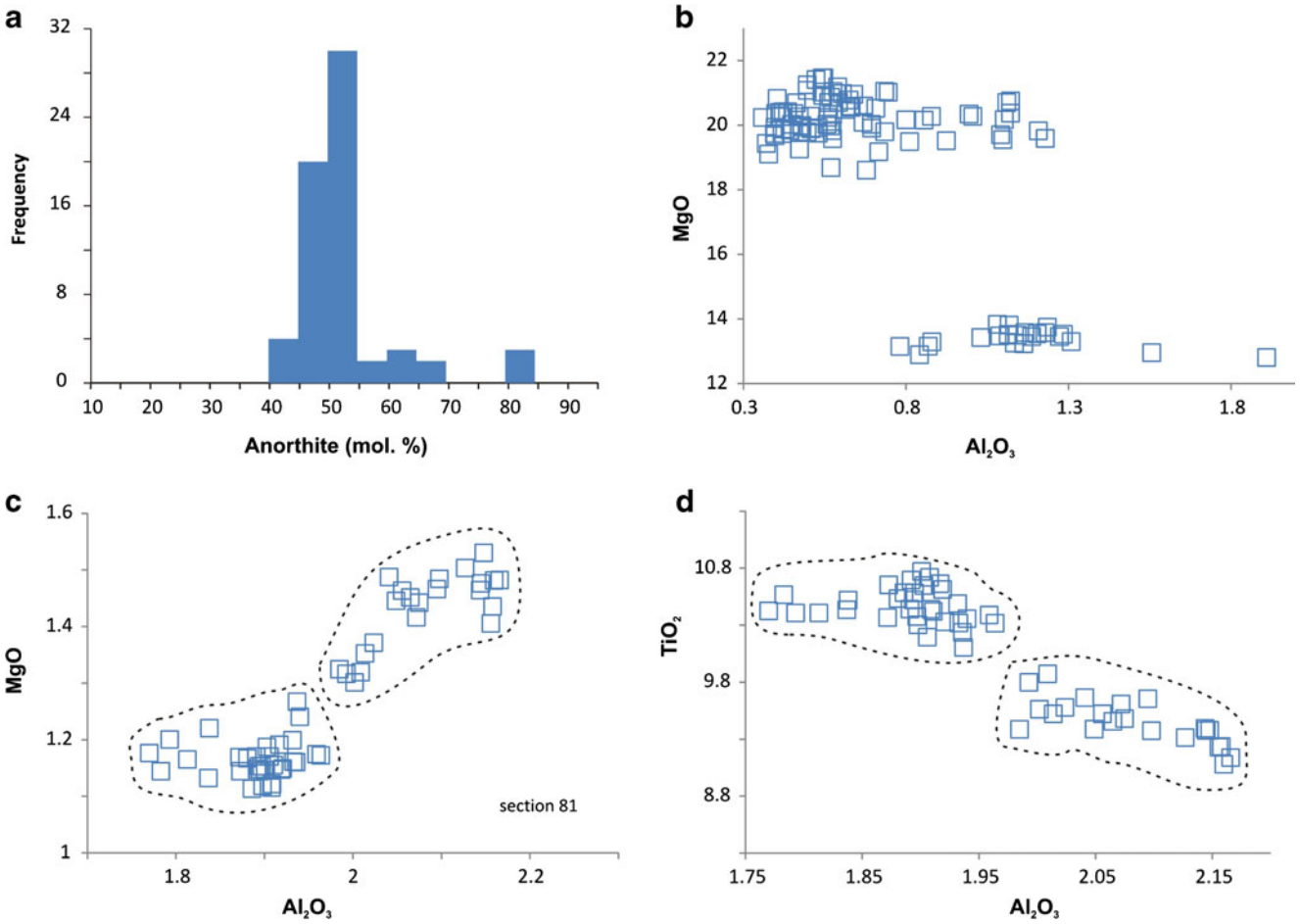

Fig. 12 **a** Compositional ranges of plagioclase populations of pumices collected at site 9 (UAq), as well as compositions of pyroxenes (**b**). Orthopyroxene has higher contents of MgO (>18 wt.%), whereas clinopyroxene groups in lower MgO<14.2 wt.% contents. Data are spread which reflects the presence of two groups of pyroxenes. **C**, **d** The compositions of titanomagnetite show two groups

Physical parameters of the eruption

Distribution

We described 44 stratigraphic profiles with detailed measurements of thickness, components, and their characteristics (Fig. 4). As shown in this figure, UAq covers large areas of Managua, Ciudad Sandino, and the Mateare escarpment. The maximum exposed thickness of UAq is 4.6 m at section 9 in Acahualinca (Figs. 4, 5, and 6a–b). Here, it is represented by a massive, framework-supported, reversely graded layer with lapilli pumice at the base and block pumice towards the top. The thinnest described UAq outcrop is 52 cm thick at section 6 in Las Colinas area (Fig. 4). South of the Mateare escarpment, UAq is 1.5 m thick on average.

To construct isopachs, we used the 44 sections described in this work and 35 sections described by Bice (1985) for a total of 79 sites (Fig. 4). There are no outcrops around Mateare village where UAq has been eroded (see Appendix A). To fill this gap, we extrapolated thicknesses of the deposit considering those found in the Nejapa Volcanic Field and along the Mateare escarpment (Fig. 4). Based on the new data, the UAq was dispersed to the south and covers a minimum area of 877 km^2 within the 50 cm isopach. The most distal exposure of UAq occurs at El Crucero 22 km from the Apoyeque volcano crater (Fig. 4).

Volume

The proximal volume was calculated by using the methods of Pyle (1989, 1995) and Fierstein and Nathenson (1992), yielding a volume of 2.3 km^3 (Fig. 4). Due to the absence of distal outcrops, we applied Eq. 18 of Fierstein and Nathenson (1992) combined with the method of Sulpizio (2005) to estimate the distal volume of the deposit based on the relationship between the distal slope (k1) and the break in slope (√Aip). The parameter √Aip=29.07 km was obtained from the empirical relationship 1 of Sulpizio (2005) and k1=0.052 with Eq. 5 of the same author. These parameters were substituted in the equation of Fierstein and Nathenson (1992), in addition to the extrapolated maximum thickness (T_o) and the distal slope (k) of Fig. 4. The distal volume obtained is 0.7 km^3 for a total

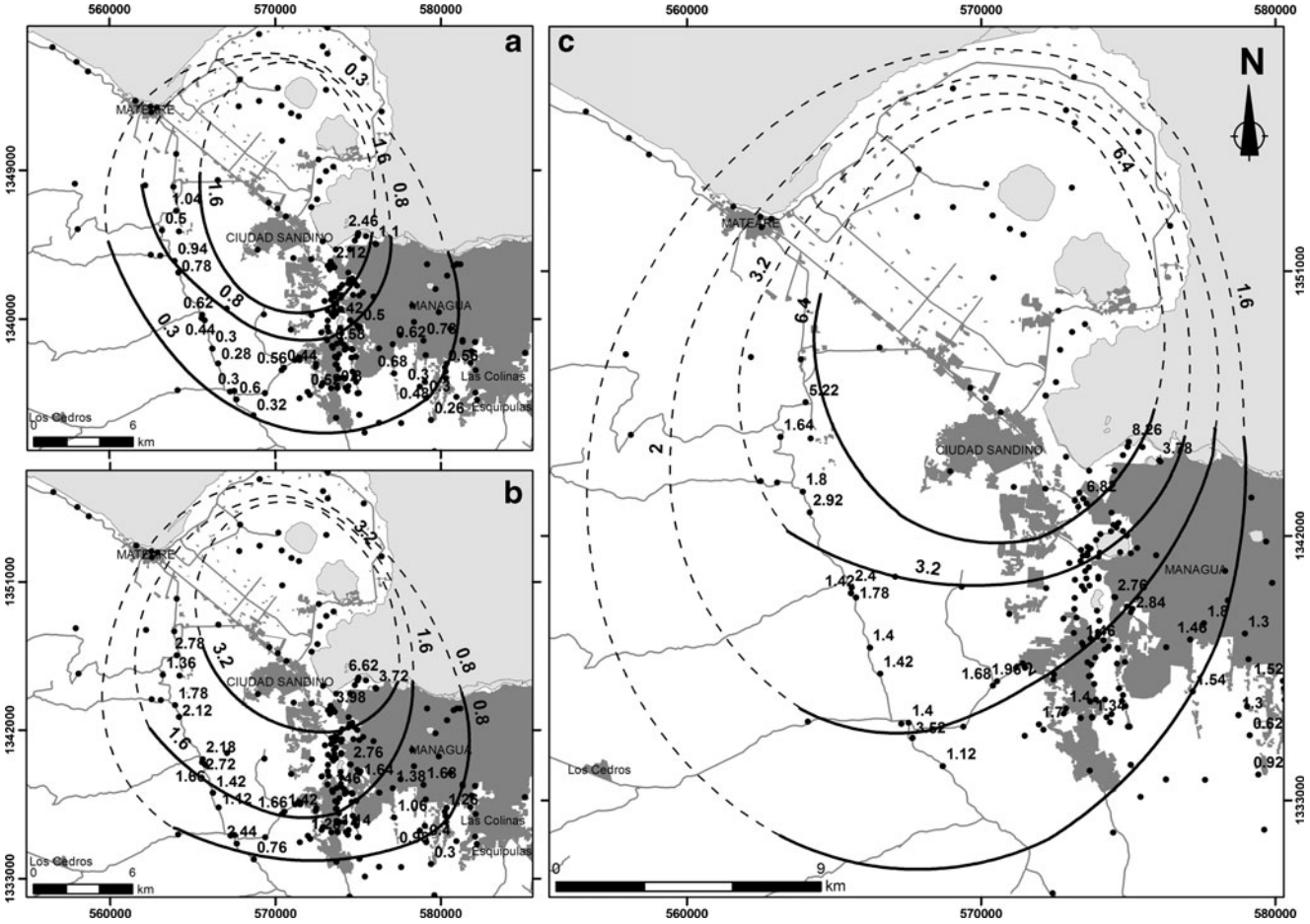

Fig. 13 Isopleth maps of the Upper Apoyeque Tephra for levels: *lower* (**a**), *middle* (**b**), and *upper* (**c**) of the stratigraphic column. These maps were constructed from the average of the five lithics measured at each section. *Contour lines* are in centimeters

volume of UAq of 3 km^3. A dense rock equivalent (DRE) of 1.15 km^3 was calculated considering an average deposit density of 1,000 kg/m^3 and a dacitic magma density of 2,600 kg/m^3.

Column height and eruption style

We used the method of Carey and Sparks (1986) to calculate eruption column height. It was applied to three different levels of the deposit (a, c, and e) where lithics are abundant. For the lowermost level-a, we used the isopleths for lithic fragments with diameters of 1.6 and 0.8 cm, resulting in column heights of ~20 and 23 km and wind speeds ~21 and 12 m/s, respectively (Figs. 13a and 14a–b). For level-c, we applied the isopleth graphs for fragments with diameters of 3.2 (~24 km column height) and diameters of 1.6 cm, obtaining a ~28.3-km-high column (Figs. 13b and 14b–c). For level-e, we used isopleth graphs for fragments with 3.2 and 6.4 cm diameters resulting in column heights of 28 and 28.3 km and wind speeds between 18 and 25 m/s, respectively (Figs. 13c and 14c–d). For comparison, we used the method of Pyle (1989) shown in Fig. 15a, from which we obtained a slope *k* value of 0.126 and the parameter of the half distance of the maximum clasts extrapolated (bc) of 3.1 km with a neutral buoyancy column height of 20 km (Fig. 15b). With these values and the approximation of HB/HT ~0.7 (Pyle 1989), we obtained a total column height of 28.6 km (Pyle 1989).

From the isopach and isopleth maps of the deposit, we calculated the bt and bc parameters of Pyle (1989) yielding values of 3.7 and 3.1, respectively. These parameters are consistent with the values expected for a Plinian eruption (Fig. 15c).

Emission rate and duration of the eruption

The emission rate was calculated with the method of Wilson and Walker (1987) by using the equation H [km]=0.236× $Mo^{1/4}$ [kg/s], where H=column height; Mo=Emission rate, and 0.236 as a constant. For the lowest level-a, we used column heights of 20 and 23 km resulting in emission rates of ~5×10^7 and 9×10^7 kg/s, respectively. For level-c, a column height of 24 km yields an estimated emission rate of ~1×10^8 kg/s, and for the uppermost level-e, a column height of 28.3 km corresponds to an emission rate of ~2×10^8 kg/s. We

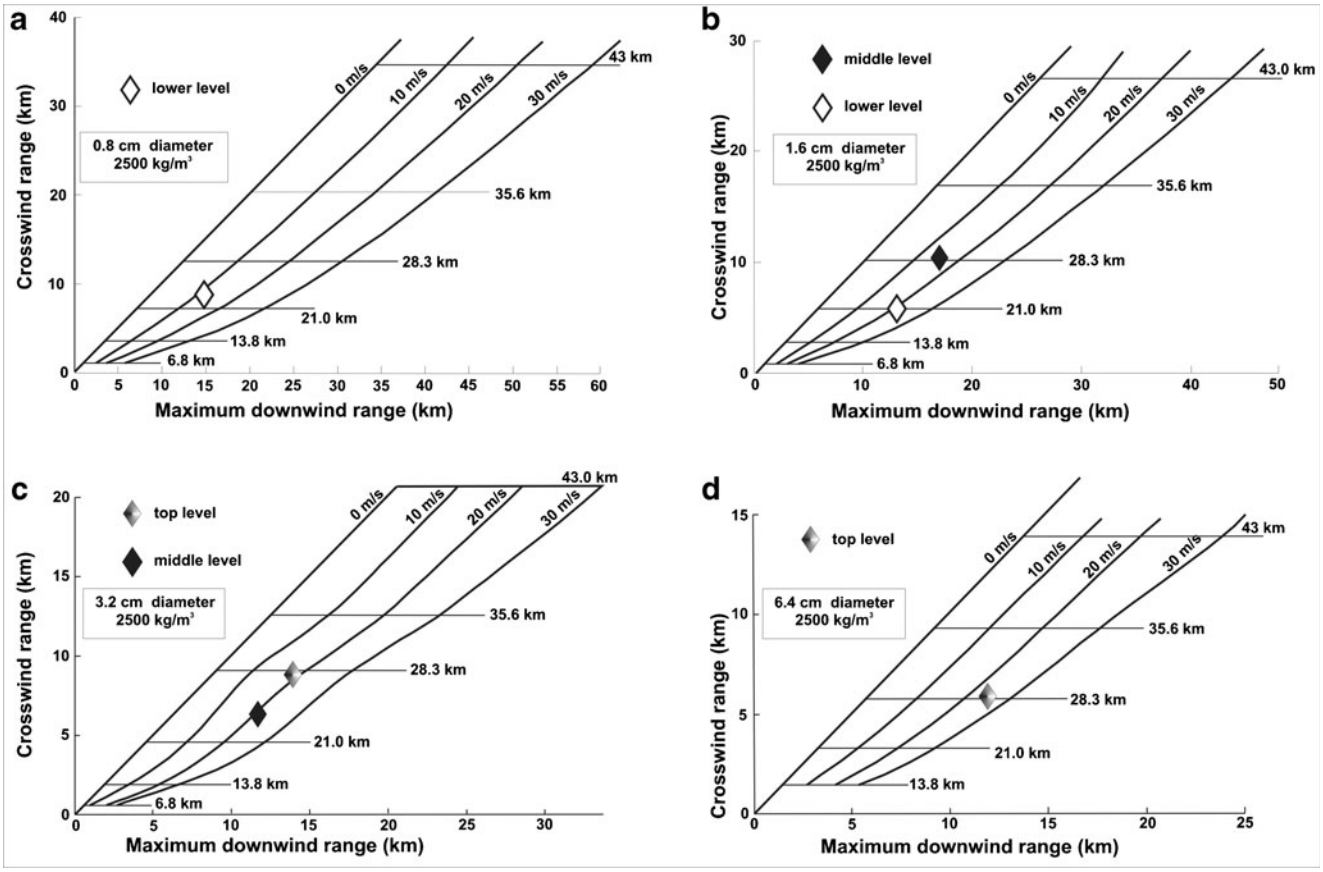

Fig. 14 Modified graphs of the maximum downwind range versus crosswind range of Carey and Sparks (1986) for different clast-sizes. **a** 0.8 cm diameter clasts of the lower part of the UAq deposit. **b** 1.6 cm diameter clasts of the lower and middle parts; **c** 3.2 cm diameter clasts of the middle and top parts. **d** 6.4 cm diameter clasts of the topmost part of the stratigraphic column

also applied the equation Ht [km]=1.67×Q0.259 [m^3/s] of Carey and Bursik (2000) where Ht=maximum height of the eruptive column; Q=volumetric emission rate; and 1.67 is the atmospheric stratification constant. Considering the maximum column height of 28.3 km, the eruption reached a maximum volumetric discharge rate of ~5.5×10^4 m^3/s. To estimate the magmatic emission rate, we interpolated the maximum column height versus the volumetric emission rate in the diagram of Carey and Bursik (2000), resulting in a comparable value of ~1×10^8 kg/s (Fig. 15d).

Based on these results, we conclude that the total emission rate was ~2×10^8 kg/s. Considering that the emission rate is controlled by the column height and the eruption dynamics (Wilson and Walker 1987), and that the numerical approximation is applicable to circular craters as the Apoyeque vent, we consider this figure a reasonable result.

To calculate the duration of the eruption, we applied the method of Wilson (1976) with the equation Te [h]=mT [kg]/m [kg/s], where: Te is the minimum theoretical duration time; mT is the total erupted mass (δ magma×DRE-volume) (dacitic magma with a density of 2,600 kg/m^3 times the DRE volume in cubic meters); and m is the emission rate. Considering a total mass of 3×10^{12} kg and an emission rate of 2×10^8 kg/s, we obtained a minimum duration time of 4 h.

Discussion

Pre-eruptive conditions and magmatic processes

Based on the model of Ridolfi et al. (2010), the amphiboles of the UAq pumice equilibrated at temperatures of 830±17 °C and pressures of 135±12 MPa. According to the calibration of Ghiorso and Evans (2008) and the test of Bacon and Hirschmann (1988), the Fe-Ti oxide pairs in equilibrium suggest a pre-eruptive temperature of 849±4 °C and an oxygen fugacity of logfO_2=NNO+0.53±0.03. Such a temperature agrees with those obtained for the amphiboles.

The lack of equilibrium in some Fe-Ti oxides and the different concentrations in Al_2O_3, MgO and TiO_2 (Fig. 12c–d) suggest mixing and/or assimilation occurred prior to eruption. Glass matrix can be lumped into two groups with different major oxide concentrations (Fig. 11). Individual plagioclase crystals contain large compositional variations (e.g., $An_{42\text{-}55}$, $An_{84\text{-}45}$, and $An_{43\text{-}83}$). Although we do not have

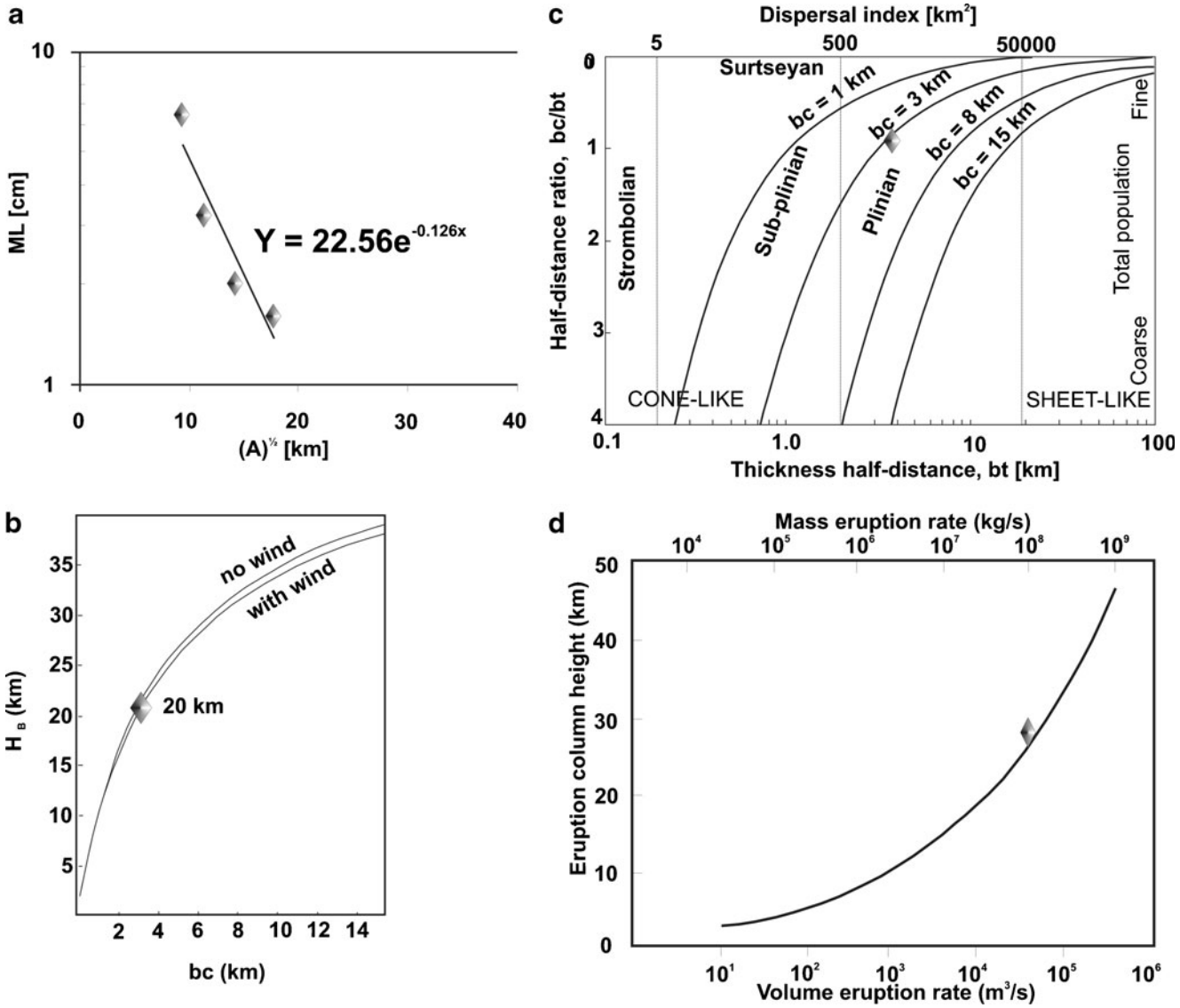

Fig. 15 **a** Square root of the isopleth area (√A) versus the average diameter lithic fragments (ML) of isopleths of the upper levels of the UAq deposit. **b** Clast half-distance (bc) versus neutral buoyancy height (HB) graph of UAq (Pyle 1989) showing the predicted column neutral buoyancy height. **c** bt versus bc/bt diagram (Pyle 1989) used to classify the eruptive style of UAq. **d** Eruption column height versus magma discharge rate of UAq (modified from Carey and Bursik 2000)

core-rim compositional transects in plagioclase and Fe-Ti oxides, such compositional variability in crystals and glass matrix can be related to magma mixing (e.g., Chertkoff and Gardner 2004; Sosa-Ceballos et al. 2012). UAq juvenile fragments do not, however, show hand specimen evidence of magma mixing (e.g., banded pumice).

Vent source

The stratigraphic characteristics of the UAq deposit in all sections described in the Managua area, supported by the isopach and isopleth maps, suggest that the most likely site of the UAq eruption is Apoyeque volcano (Figs. 4 and 13). The thickness of the deposit clearly increases from south to north up to a maximum exposed at Acahualinca (site 9), clearly pointing towards Apoyeque. The texture, modal content, and mineral paragenesis of the edifice lavas of Apoyeque are similar to the cognate lithics (gray and red-pink andesites and dacites, respectively) found in the UAq deposit. The accidental red altered lithics with basaltic compositions are related to rocks underlying the volcano. These basaltic lithics correlate with rocks belonging to lavas of Chiltepe and Xiloá scoria cones that have characteristics of rocks of the Nejapa Volcanic Field and the basaltic–andesitic lavas of Las Sierras Formation (Avellán et al. 2012). Therefore, the UAq eruption is not associated with rocks forming the Cuesta El Plomo tuff cones where Kutterolf et al. (2007) place the source of UAq. If the source were there, the accidental lithics found in the UAq

deposit would be fragments from base surge deposits that constitute these cones and of basaltic andesitic lavas belonging to Las Sierras Formation.

Eruptive mechanism

Based on the reverse grading of the deposit, texture (vesicle sizes and appearance of glomerocrysts towards the top) and gradational granulometric variations through the deposit, it is probable that the eruption occurred in three successive phases, as described below:

The initial magma expansion, acceleration, and fragmentation through the conduit established a sustained stable Plinian column with heights fluctuating between 20 and 23 km and intensities between 5×10^7 and 9×10^7 kg/s, respectively. During this first phase of the eruption, the column was influenced by dominant winds with speeds between 12 and 21 m/s. Winds dispersed the plume S–SE from the crater, producing an asymmetric ash and pumice deposit with minor lithics (5 vol.%). The plume blanketed the southern region, covering volcanic structures located along the Nejapa fault (e.g., scoria cones south of Xiloá, San Patricio, and tuff cones Cuesta El Plomo). To the SE, the plume blanketed the current urban area of Managua and the Mateare escarpment overlying either the soil at that time or older deposits produced at Apoyo and Masaya volcanoes (e.g., Apoyo and Fontana tephras, respectively). The eruption increased its energy over time, as evidenced by the increase in particle size within the UAq deposit, coupled with an increase in the lithic content (to 8 vol.%). These lithics were stripped from the volcanic vent due to erosion and enlargement of the conduit. Two hours after the beginning of the eruption, the column was 24 km high (Plinian), and the eruption had an intensity of ca. 1×10^8 kg/s, producing a shower of blocks in the proximal zones. By that time, the wind speed had decreased to 15 m/s and was dispersing the plume to the SE–SW. After 3 h, the eruption reached its maximum intensity (~2×10^8 kg/s), with a column height of up to 28 km. These conditions were reflected by a plume emplacing a larger amount of lithics (12 vol.%) and large pumice blocks (6–30 cm long) at 9 km from the source. The column was influenced by a wind speed of 18 m/s dispersing a fan-shaped symmetrical deposit, which was elongated to the south. During the last phase of the eruption, the column was dispersed by predominant winds having speeds up to 25 m/s S–SW causing deposition of ash up to 300 km over the Pacific Ocean seafloor with a minimum thickness of 1 cm (Kutterolf et al. 2008). The energy of the eruption decreased with time, leading to the deposition of coarse pumice and a slight reduction in lithic content (11 vol.%). The eruption lasted for about 4 h (based on available models, Wilson 1976).

To date, we have not found any evidence of the eruption column collapse. However, after the eruption, re-mobilization of pumice from the upper parts of the UAq generated lahars. Younger eruptions that emplaced density currents related to the phreatomagmatic eruptions of neighboring monogenetic volcanoes (e.g., Upper-Cuesta El Plomo Tuff and Nejapa Tephra dated at 7,135±125 years BP) were also able to erode the UAq deposit, with significantly scoured surfaces observed in many outcrops located at Cuesta El Plomo tuff cone and Nejapa maar. Around the volcano and in some sections south of Managua, the UAq deposit was completely eroded by lahars triggered by common heavy rains that hit the region.

Conclusions

Apoyeque volcano is now considered to be active, but quiescent. It may have begun erupting during late Pleistocene with emission of at least four lava units and domes of andesitic to dacitic compositions. The stratigraphic record indicates that Apoyeque has experienced at least three Plinian eruptions, one ~17 kyears ago (Lower Apoyeque Tephra), another at 12.4 ka (UAq eruption), and the most recent at between 1.9 and 4 ka (Chiltepe Tephra). A fourth possible Plinian eruption of Apoyeque volcano with a very similar mineral paragenesis as the UAq deposit could be represented by the W–SW dispersed fall deposit found around the town of Mateare, stratigraphically underneath the UAq deposit. All this suggests that Apoyeque activity has changed from predominantly effusive to predominantly explosive through time.

The UAq eruption was caused by a magma mixing event that produced a hybrid rhyodacitic magma. Prior to eruption, the magma was stagnant at pressures of 135 Mpa and temperatures between 830 and 849 °C. The mixing caused overpressurization of the magmatic system and fragmentation of the magma, which rapidly formed a sustained 20 km high eruptive plume. This plume grew steadily, eroding the conduit walls and reaching a maximum height of ca.28 km in less than 4 h. The eruption released homogeneous rhyodacitic pumice that was distributed to the south of the volcano (UAq). A future Plinian eruption of this magnitude could have catastrophic consequences, for more than half of the population of the city of Managua and other places as Mateare and Ciudad Sandino. Ash-fall deposits extending beyond the limits of Managua with a thickness exceeding 2 m would be enough to completely bury many houses and small buildings in the city. In addition, the re-mobilization of material and generation of lahars could also have a major impact on lower lands in the Managua graben region.

Acknowledgments We appreciate the great support of Juan Francisco Vasquez who helped us throughout the field work and the drivers Santiago Noguera and Adalberto Solórzano of the IGG-CIGEO/UNAN-Managua, Nicaragua. We thank Carlos Lineares for their support in the electron microprobe analysis at the Instituto de Geofísica, UNAM. We also thank the technical support of Fabiola Mendiola and Ana María

Rocha. This study was financially supported by PMIA (Programa Multidisciplinario de Investigación Ambiental) coordinated by Dionisio Rodríguez. We thank N. Pardo and G. Gómez for their valuable comments to the first draft of this manuscript. Careful reviews by G. Giordano, S. Cronin, and anonymous reviewer greatly improved the content of this manuscript.

Appendix A

According to Kutterolf et al. (2007), the UAq covers the Lower Apoyeque Tephra (~17 ka old) and underlies the Xiloá Tephra (Chiltepe Formation) around Mateare (Figs. 4 and 5; Sections 77, 78, and 81). However, in this area, the UAq deposit has different characteristics of those commonly observed around the Managua region finding several discrepancies mention below:

1. Stratigraphy: The reversely graded character of the UAq occurs everywhere but at Sections 77, 78, and 81 located around the Mateare village, some 10 km southwest of the Apoyeque stratovolcano. In these localities, the deposit described by these authors appears as a stratified basal layer followed by a thick massive ungraded layer (ESM 6). The stratified basal layer (55 cm of total thickness) consists of two horizons (20 cm thick each) of coarse lapilli white pumice and lithics, interbedded with three coarse ash and pumice horizons (5 cm thick each). The upper layer (~1 m thick) is a massive coarse-clast supported and consists of coarse lapilli to block-sized white pumice, lithics, and white banded pumice (light-gray stripes). This massive layer does not show reverse grading. Kutterolf et al. (2007) concluded that these deposits belong to the UAq and referred this change in lithofacies as due to proximal sedimentation and wet emplacement of the tephra fallout in the Xolotlan lake shore. After which, they were covered by the sedimentation of the massive upper part.
2. Age: Two other paleosol samples were collected at site 77, located at 3 km of the Mateare locality, along the New Road to León (Fig. 4). These paleosol were collected at the base and at the top of the pyroclastic deposit reported by Kutterolf et al. (2007) as the UAq deposit. Both samples were analyzed at the same laboratory by using the ^{14}C AMS-standard radiometric method. The paleosol at the base of the fall deposit is thin (5 cm thick), light-brown, silty, and humic-poor. The thin paleosol was developed from lake sediments related to a tsunami deposit identified by Freundt et al. (2006). The age obtained for this basal paleosol was 4,350±30 years B.P. being younger and unreliable according to the stratigraphic position. The paleosol on top developed from the fall deposit is dark-brown, clayey-silty, with a moderate content of humic material. A sample taken from the uppermost 5-cm paleosol yielded an age of 12,130±50 years B.P. suggesting that this fall deposit is older. This age is around 100 years younger than the UAq dated at 12,400±100 years B.P (Kutterolf et al. 2007) and 12,285+280/−270 years B.P. (this work). We propose that at site 77 and other locations around the Mateare village, the UAq fallout was eroded by pyroclastic surges of the Xiloá eruption.
3. Petrography: At site 81, some hand specimens of pumice are banded with white and narrow gray bands. In thin section, the pumice is heterogeneously vesicular (highly to slightly), with fibrous patches. The vesicles have different shapes varying from dominantly elongated to semi-rounded. The mineral paragenesis of the pumice samples at Section 81 is similar to UAq.
4. Chemistry: Two additional samples of pumice (base=*ax* and top=*ex*) were collected at Section 81 around Mateare (described by Kutterolf et al. 2007) to compare their mineralogy and chemistry with samples of Section 9 (ESM 7 and 8). Such comparison was made to corroborate the UAq deposit features observed in the field, its stratigraphic position, and distribution around the source. The chemistry of 81 (Mateare) are very similar in bulk composition (66.9–68.5 wt%) straddling the dacitic–rhyolitic fields. The groundmass glass composition of pumice clasts in Section 81 (Mateare) is also rhyolitic but clustered at lower silica contents (71.38±0.9 wt%) and is more heterogeneous.

Discussion

Several lines of evidence suggest that the deposit described by Kutterolf et al. (2007) around Mateare does not correspond to the UAq deposit widely dispersed around Managua, as described by Bice (1985) and in this study. These evidences are (a) the basal-stratified layers described in Mateare do not occur in any other exposure of UAq around Managua, (b) the massive upper part at Mateare does not show the distinctive reverse grading of pumice and lithics that are ubiquitous of UAq, and (c) the deposit at Mateare contains rare white-banded pumice with light-gray stripes that do not occurred in the UAq deposit.

The age span and uncertainties obtained for these two eruptions do not allow to clearly separating them in time. However, the structure of the deposit, componentry, and mineral chemistry (glass, oxide, and plagioclase compositions) (ESM 7 and 8) shown above indicate that the UAq deposit is different from the fall deposit described at Mateare by Kutterolf et al. (2007). We proposed that the volcano generated two different eruptions closely separated in time (~100 years apart), an older one dispersed to the southwest

and a younger one (UAq) dispersed to the south. If this is the case, UAq was eroded by pyroclastic or sub-aerial processes around Mateare.

At site 81 (Mateare), the pumice sample has a very similar mineral composition of pyroxene ($En_{58–63}$, $Fs_{35–40}$, $Wo_{2–3}$, and Mg#=45–50) and amphiboles (temperatures of 830± 11 °C and equilibrium pressures of 130±9 MPa; Ridolfi et al. 2010). However, plagioclase is variable in composition (An_{43} to An_{72}). It was not possible to find ilmenite even in mineral separates. In contrast to the UAq Fe–Ti oxides, the Mateare pumice clasts plot in a single titanomagnetite group with Al_2O_3 (2.05–2.18 wt%), MgO (1.27–1.55 wt%), and with a lower TiO_2 content (8.5–9.3 wt%). These marked differences further confirm that pumice of Mateare is definitely different to the UAq deposit.

References

Avellán DR, Macías JL, Pardo N, Scolamacchia T, Rodríguez D (2012) Stratigraphy, geomorphology, geochemistry and hazard implications of the Nejapa Volcanic Field, western Managua, Nicaragua. J Volcanol Geotherm Res 213–214:51–71

Bice DC (1985) Quaternary volcanic stratigraphy of Managua, Nicaragua: correlation and source assignment for multiple overlapping plinian deposits. Geol Soc Am Bull 96:553–566

Bacon CR, Hirschmann MM (1988) Mg/Mn partitioning as a test for equilibrium between coexisting Fe-Ti oxides. Am Mineral 73:57–61

Carey S, Sparks RSJ (1986) Quantitative models of the fallout and dispersal of tephra from volcanic eruption columns. Bull Volcanol 48:109–125

Carey S, Bursik M (2000) Volcanic plumes. In: Sigurdsson H, Houghton BF, McNutt SR, Rymer H, Stix J (eds) Encyclopedia of volcanoes. Academic, San Diego, pp 527–544

Chertkoff DG, Gardner JE (2004) Nature and timing of magma interactions before, during, and after the caldera-forming eruption of Volcán Ceboruco, Mexico. Contrib Mineral Petrol 146:715–735

DeMets C (2001) A new estímate for present-day Cocos-Caribbean plate motion: implications for slip along the Central America volcanic arc. Geophys Res Lett 28:4043–4046

Fierstein J, Nathenson M (1992) Another look at the calculation of tephra fallout volumes. Bull Volcanol 54:156–167

Freundt A, Kutterolf S, Wehrmann H, Schmincke HU, Strauch W (2006) Eruption of the dacite to andesite zoned Mateare Tephra, and associated tsunamis in Lake Managua, Nicaragua. J Volcanol Geotherm Res 149:103–123

Gardner JE, Thomas RME, Jaupart C, Tait S (1996) Fragmentation of magma during Plinian volcanic eruptions. Bull Volcanol 58:144–162

Ghiorso MS, Evans BW (2008) Thermodynamics of rhombohedral oxide solid solutions and a revision of the Fe-Ti two oxide geothermometer and oxygen barometer. Am J Sci 308:957–1039

Houghton BF, Wilson CJN (1989) A vesicularity index for pyroclastic deposits. Bull Volcanol 51:451–462

Inman DL (1952) Measures of describing the size distribution of sediments. J Sed Petrol 22:125–145

Kutterolf S, Freundt A, Pérez W, Wehrmann H, Schmincke HU (2007) Late Pleistocene to Holocene temporal succession and magnitudes of highly-explosive volcanic eruptions in west-central Nicaragua. J Volcanol Geotherm Res 163:55–82

Kutterolf S, Freundt A, Peréz W, Mörz T, Schacht U, Wehrmann H, Schmincke HU (2008) Pacific offshore record of plinian arc volcanism in Central America: 1. Along-arc correlations. Geochem Geophys Geosyst 9:Q02S01. doi:10.1029/2007GC001631

Pardo N, Avellán DR, Macías JL, Scolamacchia T, Rodríguez D (2008) The 1245 yr BP Asososca maar: new advances on recent volcanic stratigraphy of Managua (Nicaragua) and hazard implications. J Volcanol Geotherm Res 176(4):493–512

Pyle DM (1989) The thickness, volume and grain size of tephra fall deposits. Bull Volcanol 51:1–15

Pyle DM (1995) Assessment of the minimum volume of tephra fall deposits. J Volcanol Geotherm Res 69:379–382

Ridolfi F, Renzulli A, Puerini M (2010) Stability and chemical equilibrium of amphibole in calk-alkaline magmas: an overview, new thermobarometric formulations and application to subduction-related volcanoes. Contrib Mineral Petrol 160:45–66

Shand SJ (1951) Eruptive rocks. Wiley, New York, pp 1–488

Sosa-Ceballos G, Gardner JE, Siebe C, Macías JL (2012) A caldera-forming eruption ~14,100 14C yr BP at Popocatépetl volcano, México: insights from eruption dynamics and magma mixing. J Volcanol Geotherm Res 213–214:27–40

Sparks RSJ (1978) The dynamics of bubble formation and growth in magmas: a review and analysis. J Volcanol Geotherm Res 3:1–37

Sulpizio R (2005) Three empirical methods for the calculation of distal volume of tephra-fall deposits. J Volcanol Geotherm Res 145:315–336

Walther CHE, Flueh ER, Ranero CR, von Huene R, Strauch W (2000) Crustal structure across the Pacific margin of Nicaragua: evidence for ophiolitic basement and a shallow mantle sliver. Geophys J Int 141:759–777

Wilson L (1976) Explosive volcanic eruptions-III. Plinian eruption columns. Geophys J Res Astron Soc 45:543–556

Wilson L, Walker GPL (1987) Explosive volcanic eruptions-VI. Ejecta dispersal in plinian eruptions: the control of eruption conditions and atmospheric properties. Geophys J Res Astron Soc 89:657–679

Wohletz K (2006) KWare SFT. Sequential fragmentation/transport models. Version 2.19.0165, Los Alamos Lab, University of California